

RESEARCH

A suppressor of dioxygenase inhibition in a yeast model of SDH deficiency

William Beimers*^{ORCID}, Megan Braun*, Kaleb Schweinfus, Keenan Pearson, Brandon Wilbanks and Louis James Maher^{ORCID}

Department of Biochemistry and Molecular Biology, Mayo Clinic College of Medicine and Science, Rochester, Minnesota, USA

Correspondence should be addressed to L J Maher: maher@mayo.edu

*(W Beimers and M Braun contributed equally to this work)

Abstract

A fascinating class of familial paraganglioma (PGL) neuroendocrine tumors is driven by the loss of the tricarboxylic acid (TCA) cycle enzyme succinate dehydrogenase (SDH) resulting in succinate accumulation as an oncometabolite and other metabolic derangements. Here, we exploit a *Saccharomyces cerevisiae* yeast model of SDH loss where accumulating succinate, and possibly reactive oxygen species, poison a dioxygenase enzyme required for sulfur scavenging. Using this model, we performed a chemical suppression screen for compounds that relieve dioxygenase inhibition. After testing 1280 pharmaceutically active compounds, we identified meclofenoxate HCl and its hydrolysis product, dimethylaminoethanol (DMAE), as suppressors of dioxygenase intoxication in SDH-loss yeast cells. We show that DMAE acts to alter metabolism so as to normalize the succinate:2-ketoglutarate ratio, improving dioxygenase function. This study raises the possibility that oncometabolite effects might be therapeutically suppressed by drugs that rewire metabolism to reduce the flux of carbon into pathological metabolic pathways.

Key Words

- ▶ succinate dehydrogenase
- ▶ *Saccharomyces cerevisiae*
- ▶ paraganglioma
- ▶ drug screen

Endocrine-Related Cancer
(2022) **29**, 345–358

Introduction

Metabolic dysregulation underlies many diseases. Cancer was characterized by a metabolic perturbation now known as the Warburg effect, the observation that cancer cells exhibit glycolytic, rather than oxidative, metabolism even when oxygen is abundant (Warburg 1956). Since this discovery, many cancers have been found to have other forms of altered metabolism besides the Warburg effect (Pavlova & Thompson 2016, Kozal *et al.* 2021). Familial paraganglioma (PGL) is a remarkable example. PGL is a rare neuroendocrine tumor affecting between 1:100,000 and 1:300,000 people (Erickson *et al.* 2001, Berends *et al.* 2018). The most common form of PGL arises in the chromaffin cells that make up the adrenal medulla, which is known as pheochromocytoma (Lenders *et al.* 2005). PGL can be

characterized by hypertension due to the secretion of catecholamines, though most cases are asymptomatic. PGL is typically a slow-growing tumor and many cases are benign and are curable by surgery. About 25% of PGL cases are hereditary, and most hereditary PGLs are linked to pathogenic variants in nuclear genes encoding the four subunits of the tricarboxylic acid (TCA) cycle enzyme succinate dehydrogenase (SDH; also complex II of the electron transport chain). Such familial SDH-loss PGL cases thus involve mutations in *SDHA*, *SDHB*, *SDHC*, *SDHD* genes, and in *SDHAF2*, the nuclear gene encoding the factor required for flavin assembly in SDHA. For unknown reasons, variants in *SDHB* are mostly penetrant (Baysal *et al.* 2000, Niemann & Müller 2000, Astuti *et al.* 2001,

Hao *et al.* 2009, Burnichon *et al.* 2010). Mutations are inherited as heterozygous loss-of-function alleles, and tumorigenesis is believed to depend upon sporadic mutational loss or silencing of the remaining gene copy in chromaffin cells. Why tumorigenesis is limited to a particular cell type is also unknown.

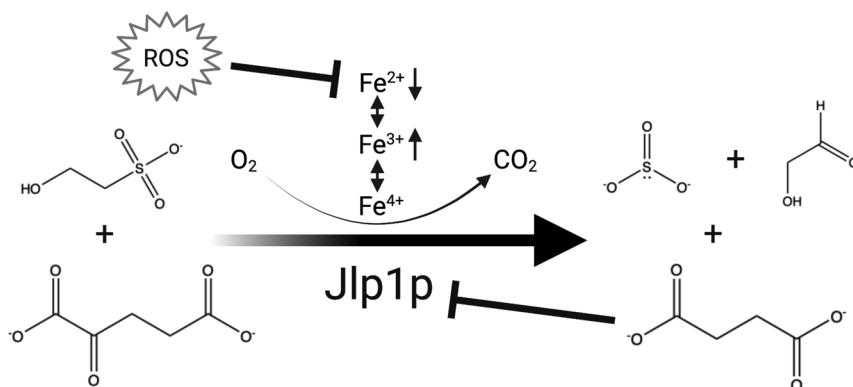
It is believed that SDH loss of function drives metabolic reprogramming leading to tumorigenesis, but the direct links between SDH loss and transformation are still being established. Current hypotheses focus on the roles of accumulating succinate as an oncometabolite, augmented damage by reactive oxygen species (ROS), and hypersuccinylation (Ishii *et al.* 2005, Selak *et al.* 2005, Smestad *et al.* 2018). ROS production has been shown to increase in SDH loss model organisms, but it is unclear how much protein and DNA damage results (Adachi *et al.* 1998, Ishii *et al.* 2005, Smith *et al.* 2007, Braun *et al.* 2019). Recent work has shown that the loss of SDHB in particular disrupts iron homeostasis, leading to exacerbated ROS generation and hallmarks of the tumor phenotype such as pseudohypoxia and DNA hypermethylation. There is evidence that this inherent oxidative stress enhances PGL sensitivity to additional oxidative damage caused by pro-oxidant compounds (Liu *et al.* 2020, Goncalves *et al.* 2021). Building on this, it is becoming clear that lack of iron homeostasis can have a role in tumor development and in the epithelial–mesenchymal transition. Notably, iron directly regulates 2-ketoglutarate levels, leading to changes in dioxygenase activity (Müller *et al.* 2020).

Succinate accumulation is an intriguing hypothesis to explain tumorigenesis, with many studies attempting to unravel mechanistic details. SDH loss presumably reprograms central metabolism toward glycolysis because SDH loss breaks the conventional TCA cycle and may alter the flow of high-energy electrons into the electron transport chain. Loss of any SDH subunit is believed to disrupt the function of the entire SDH complex. This could result in an ‘obligatory Warburg effect’ with higher dependence on glycolysis and an accumulation of succinate due to the inability of the nonfunctional SDH to produce fumarate in the TCA cycle (Her & Maher 2015). However, there is also evidence that chromaffin cells may generate ATP from residual steps within the TCA cycle and electron transport chain (Ključková *et al.* 2020). Succinate accumulation may extend as well to succinyl-CoA accumulation (one step earlier in the TCA cycle) leading to protein hypersuccinylation (Li *et al.* 2015, Smestad *et al.* 2018). The full effects of lysine succinylation on protein function remain incompletely explored. In mammalian cells, succinate also acts as a signaling

molecule to stress responses. These can include cancer-promoting behaviors such as immunosuppression and cell migration (Matlac *et al.* 2021). Crucially, accumulated succinate is a competitive inhibitor of an important class of 2-ketoglutarate-dependent dioxygenases. These iron-dependent enzymes oxygenate a substrate by splitting molecular dioxygen. In the process, the 2-ketoglutarate (2KG) co-reactant is converted to a succinate byproduct (Loenarz & Schofield 2011). Accumulated succinate can bind in the enzyme active site, inhibiting such dioxygenases and preventing important chemical transformations in cells (Koivunen *et al.* 2007, Cervera *et al.* 2009, Xiao *et al.* 2012, Letouzé *et al.* 2013, Peters *et al.* 2015). A greater understanding of the relationship between succinate accumulation and tumorigenesis is the goal of many studies, but a lack of animal models and PGL cell lines continues to challenge progress.

In an attempt to envision therapeutics and probe PGL mechanisms, several model systems, including *Caenorhabditis elegans*, zebrafish, rodents, mammalian cell lines, and the yeast *Saccharomyces cerevisiae*, have been used *in lieu* of conventional cancer models (Smith *et al.* 2007, Bancos *et al.* 2013, Smestad *et al.* 2017, Lussey-Lepoutre *et al.* 2018, Braun *et al.* 2019, Dona *et al.* 2021). Yeast models of PGL have exploited the conserved mitochondrial role of SDH for studies of metabolic disorders (Smith *et al.* 2007, Kregiel 2012, Bancos *et al.* 2013, Lussey-Lepoutre *et al.* 2018). *S. cerevisiae* offers many advantages as a model organism, including its fully sequenced genome and rich genetics (Goffeau *et al.* 1996, Feyder *et al.* 2015). The ease of laboratory maintenance and well-documented techniques for yeast analysis makes it well-suited for high-throughput assays as well (Bancos *et al.* 2013). Haploid SDH subunit deletion strains are readily available, and yeast show profound succinate accumulation upon SDH loss, as do mammalian cells (Feyder *et al.* 2015, Smestad *et al.* 2018).

Yeast also encode 2-ketoglutarate-dependent dioxygenases and can therefore serve as a model for succinate accumulation and the subsequent inhibition of these enzymes in this class (Zhang *et al.* 2020). One dioxygenase, in particular, Jlp1p (Fig. 1), is required for sulfur scavenging, converting sulfonates (such as isethionate, ISE) into readily metabolizable sulfites (Hogan *et al.* 1999). Because Jlp1p is a 2-ketoglutarate-dependent dioxygenase, it can be inhibited by excess succinate. When ISE is the only sulfur source, Jlp1p becomes an essential enzyme for growth. This allows Jlp1p function to be easily monitored simply by assaying cell growth as optical density change over a specified time. In our previous study, we found that a *jlp1Δ* strain is disabled for growth on ISE

**Figure 1**

Dioxygenase inhibition in SDH-mutant yeast. Jlp1p dioxygenase conversion of 2KG and sulfonate (ISE) into bioavailable sulfite, with succinate and an aldehyde (glycolaldehyde in this case) as byproducts. The reaction uses molecular oxygen and an enzyme-bound Fe^{2+} ion that undergoes REDOX cycling. In SDH-loss cells, both ROS and succinate accumulate. Depicted are possible mechanisms of Jlp1p inhibition under such conditions. Accumulated succinate causes competitive inhibition at the enzyme active site. Increased ROS depletes Fe^{2+} , inhibiting dioxygenase activity.

medium, as expected (Smith *et al.* 2007). Interestingly, *sdh* Δ strains are also partially disabled for growth on ISE, consistent with Jlp1p inhibition by excess succinate. In contrast, *jlp1* Δ and *sdh* Δ strains grow equally well on ammonium sulfate (AS), a sulfur source whose utilization does not require Jlp1p activity (Smith *et al.* 2007).

We reasoned that the dependence of yeast on Jlp1p activity in the presence of ISE as a sole sulfur source would provide the potential for a chemical suppression screen to identify compounds capable of mitigating Jlp1p inhibition when SDH is lost. Such compounds might act by reducing succinate accumulation or by moderating ROS production that could inhibit Jlp1p through oxidation of the Fe^{2+} ion required for catalysis (Fig. 1). It has been shown that a reduction in the levels of Fe^{2+} due to the Fenton reaction can lower dioxygenase activity (Gerald *et al.* 2004, Goncalves *et al.* 2021). Based on this concept, we report the results of a screen of the 1280-compound LOPAC library (Sigma #LO1280) and focus on the analysis of one particularly interesting compound, meclofenoxate, and its derivative, dimethylaminoethanol (DMAE), as leads that suppress Jlp1p poisoning in SDH-loss yeast strains. To the extent that SDH-loss yeast mimic the stresses of SDH-loss human tumors, meclofenoxate, and DMAE exemplify a class of compounds that might suppress tumorigenic dysfunction in SDH-loss cells by rewiring metabolism to reduce the flux of carbon into pathological metabolic pathways.

Materials and methods

Yeast strains

S. cerevisiae *sdh1* Δ , *sdh2* Δ , *jlp1* Δ strains and their WT parent BY4742 (MAT α *his3* Δ 1 *leu2* Δ 0 *lys2* Δ 0 *ura3* Δ 0) were kindly provided by David Katzmann. Strains were maintained on YPGal agar plates (1% yeast extract, 2% peptone, 2%

galactose, 2% agar, all (w/v)) and YPGal liquid media (1% yeast extract, 2% peptone, 2% galactose, all (w/v)) at 25°C. Most growth experiments were performed using minimal medium supplemented with 20 μM AS or ISE as indicated (Supplementary Table 1, see section on supplementary materials given at the end of this article; (Cherest and Surdin-Kerjan 1992)).

Yeast genotyping

Yeast genotyping was performed as described in Supplementary methods by growing cultures (5 mL) to saturation in YPD (1% yeast extract, 2% peptone, 2% dextrose, all (w/v)) at 30°C with shaking at 250 rpm.

LOPAC screen

The Library of 1280 Pharmacologically Active Compounds (Sigma #LO1280) was plated by the Institute for Therapeutics Discovery and Development at the University of Minnesota – Twin Cities. 200 nL of 10 mM stock of each compound in DMSO were deposited into each well of a 96-well polystyrene plate (Corning #3595). Additional wells received 200 nL of DMSO to serve as controls. For the screen, 200 μL of *sdh1* Δ yeast culture grown to 0.1 OD₆₀₀ in minimal medium containing 20 μM ISE as sulfur source were added to each well (so final compound concentration was 10 μM) and growth was monitored at 600 nm in a plate reader over the course of 24 h at 30°C with constant shaking at 250 rpm. The screen was accomplished with 16 96-well plates.

The power of the chemical screen setup was measured using a conventional Z score (see below). Growth of WT yeast in ISE media was compared to the growth of *sdh1* Δ and *sdh2* Δ strains by Z score calculation at multiple time points over the course of 24 h. At each point, the Z score was greater than 0, indicating the difference in growth between WT and SDH-loss strains was compatible with a

chemical screen. Potential hits were subsequently judged by calculating a Z score according to Eq. 1:

$$Z = 1 - \frac{3 * (\sigma_p + \sigma_n)}{|\mu_p - \mu_n|} \quad (1)$$

where σ_p is the s.d. of experimental growth wells (the *sdh1Δ* yeast strain grown in ISE minimal medium in wells with treatment) and σ_n is the s.d. of negative control growth wells (the *sdh1Δ* strain grown in ISE minimal medium in wells with vehicle). μ_p and μ_n are the corresponding means of experimental growth wells or negative control growth wells (Zhang *et al.* 1999). Because each screened compound provided data for a single well vs 4 data points for the control, the s.d. of the control was used as a mock parameter for the experimental s.d. in the calculation. Potential hits were identified among compounds that stimulated *sdh1Δ* growth with a Z score greater than zero. Compounds formulated with sulfate ions were excluded from consideration as they provided alternative sources of metabolizable sulfur that bypass the reliance on Jlp1p activity.

Yeast growth assay

WT, *sdh1Δ*, *sdh2Δ*, and *jlp1Δ* strains were grown overnight at 30°C in 10 mL YPGal with shaking at 250 rpm. Cultures were then diluted and grown to mid-log phase. Equal numbers of cells of each strain were harvested and washed three times with water by centrifugation at 2500 g. Cells from WT, *sdh1Δ*, *sdh2Δ*, and *jlp1Δ* strains were resuspended in minimal media supplemented with either AS or ISE (20 μM final concentration) to an OD₆₀₀ of 0.1. Yeast culture (100 μL) was pipetted into each well along with 100 μL of vehicle or drug identified as a hit in the LOPAC screen to a starting OD₆₀₀ of 0.05. Each condition was performed with four technical replicates. The growth assay was performed in a 96-well clear plate (Corning #3595) using a SpectraMax Plus 384 UV/Vis cuvette/microplate reader (Molecular Devices; San Jose, CA). The plate was loaded onto the reader and kept at 30°C without shaking with readings taken every 30 min for 24 h. Aeration was deemed adequate as the oxygen-dependent Jlp1p-catalyzed processing of ISE to sulfite was supported in WT cells. As described, yeast formed a uniform lawn at the bottom of each well for OD₆₀₀ readings (Hung *et al.* 2018). Growth effect of drug was measured by percent growth difference between treated and untreated at the end of the 24 h growth period. Hits were judged on the magnitude of the effect on *sdh1Δ* and

sdh2Δ vs WT and *jlp1Δ*. Error was calculated in R through quadruplicate technical replicates using a one-way ANOVA with a *post hoc* Tukey's HSD test for significance. Growth curves were generated in R and data were analyzed using Microsoft Excel and R.

Metabolite analysis

WT, *sdh1Δ*, and *sdh2Δ* strains were grown in triplicate for 24 h in 10 mL ISE minimal media cultures supplemented with 100 μM DMAE (Sigma, 471453-100ML). After 24 h, four OD₆₀₀ units of each sample were harvested and media was saved for analysis. Cells were washed by centrifugation twice with PBS, then resuspended in 400 μL of H₂O containing 30 μL of concentrated HClO₄. This cell suspension was vigorously agitated for 25 s and subjected to three freeze/thaw cycles on dry ice to promote cell lysis. Cell debris was removed by centrifugation and the lysate was collected and neutralized with 170 μL of 2M KHCO₃ on ice for analysis as described in Supplementary methods.

Mitochondrial purification and proteomic analysis

WT, *sdh1Δ*, and *sdh2Δ* yeast strains were grown in triplicate to saturation in 1 L cultures at 30°C with shaking at 250 rpm. Isolation of mitochondria was performed as described from 8 g wet weight yeast (Gregg *et al.* 2009) and proteomic analysis was conducted as described in Supplementary methods.

Western blotting

WT, *sdh1Δ*, and *sdh2Δ* strains were grown in 10 mL cultures in minimal media supplemented with 20 μM ISE for 24 h at 30°C with shaking at 250 rpm. Samples were pelleted by centrifugation at 2500 g and washed in DTT buffer (100 mM Tris pH 9.4, 10 mM DTT), then resuspended in 100 μL zymolyase buffer (1 M sorbitol, 20 mM Tris pH 7.5, 50 mM EDTA, 1% β-mercaptoethanol (v/v), 1–2 mg/mL Zymolyase (AMS BIO, 120493-1)) for lysis at 30°C for 15 min. Resulting spheroplasts were pelleted by centrifugation at 2000 g and resuspended in chilled lysis buffer (2% Triton X-100 (v/v), 1% SDS (w/v), 100 mM NaCl, 10 mM Tris pH 8, 1 mM EDTA) and 50 μL of chilled glass bead were added. Samples were subjected to three to five cycles of vortex mixing (1 min per cycle) with storage on ice between rounds. Samples were subjected to centrifugation at 14,000 g and the supernatant was stored at –80°C or collected for protein quantification using a BCA assay kit according to the

manufacturer's instructions (ThermoFisher 23227). Equal volumes of whole-cell protein extract were subjected to electrophoresis through denaturing 10% bis-Tris polyacrylamide gels and transferring to PVDF membrane. Equal loading was demonstrated by staining in parallel using Coomassie blue (BioRad). After blocking (5% non-fat dry milk (w/v), Tris-buffered saline, 1% Tween 20 (v/v)), membranes were probed with rabbit polyclonal anti-pan-succinyl lysine antibody (PTM Biolabs, PTM-401) at a dilution of 1:1000. Membrane was washed and incubated with IRDye® 800CW goat anti-rabbit IgG secondary antibody (Licor, 926-32211) and imaged using an Amersham Typhoon instrument.

Fluorescence microscopy

For live-cell detection and quantitation of ROS, cells were grown in minimal media (10 mL) at 30°C with shaking at 250 rpm for 24 h to mid-log phase (0.5 OD₆₀₀). ROS were detected by including H₂DCF-DA (ThermoFisher #D399) at a final concentration of 10 µM during the 24 h incubation. Dihydroethidium (DHE) ROS detection was performed according to previously published methods (Liao *et al.* 2020). Cells were then harvested as 1 mL at a time, subjected to centrifugation at 10,000 g, and washed three times with H₂O. The resulting cell pellet was resuspended in 20 µL of H₂O and 5 µL was pipetted onto a glass microscope slide and spread into a thin layer with a glass coverslip. Images were captured at room temperature using an Olympus IX70-S1F2 fluorescence microscope equipped with an Olympus UPlanApo 100× numerical aperture in 1.35 oil objective with the complementing immersion oil ($n = 1.516$, Applied Precision, Issaquah, WA), Standard DeltaVision filters FITC and Rhodamine and Photometrics CoolSNAP HQ CCD monochrome camera (Teledyne photometrics, Tucson, AZ). Image was acquired using Delta Vision softWoRx (version 3.5.1, Applied Precision, Issaquah, WA) and subsequently processed by Fiji (version: 2.1.0/1.53c, NIH). Captured images were exported under the standard DeltaVision file format and converted into 16-bit TIFF images by using Bio-Formats Importer available within Fiji. The contrast and brightness of images were subsequently adjusted within Fiji as well. Data represent quantification from a minimum of three independent labeling experiments with each experiment quantified at least 30 cells. Average cellular fluorescence was quantified using CellProfiler software. Statistical significance was assessed in R by a two-way ANOVA with a *post hoc* Tukey HSD test.

Protein carbonyl colorimetric assay

Protein carbonyl levels in yeast whole-cell lysates were assessed using a colorimetric assay (Sigma-Aldrich, MAK094). WT, *sdh1Δ*, and *sdh2Δ* strains were grown in 10 mL minimal media cultures supplemented with ISE (20 µM) with or without indicated concentrations of DMAE for 24 h at 30°C with shaking at 250 rpm. Protein lysates were prepared as described for Western blotting. Carbonyl levels were assayed according to manufacturer's instructions. Data analysis was performed in Microsoft Excel. Statistical significance was assessed in R by a two-way ANOVA with a *post hoc* Tukey HSD test in R.

Results and discussion

Yeast strain characterization

As the present study was based on the previous work of Smith *et al.* (2007), we began by validating the four experimental yeast strains (WT, *sdh1Δ*, *sdh2Δ*, and *jlp1Δ*) required for interpreting chemical suppression screen results. PCR genotyping confirmed the identity of each strain (Supplementary Fig. 1). Growth testing was performed in AS and ISE minimal galactose liquid media to avoid glucose repression while still enabling fermentation and oxidative metabolism (Kayikci & Nielsen 2015).

When oxygen is available, *S. cerevisiae* cells grow preferentially by fermentation until fermentable substrates are depleted. A transition to oxidative metabolism then occurs to metabolize the products of fermentation. This transition is evidenced by a diauxic shift and growth deceleration between two distinct periods of growth. Absence of this diauxic shift suggests glycolytic growth without transition to oxidative metabolism. For example, growth curves for the four yeast strains in this study (Fig. 2A and B) reveal the presence of an expected diauxic shift in the WT and *jlp1Δ* strains in AS medium, indicating sufficient oxygen and an intact TCA cycle and electron transport chain for oxidative growth. In contrast, SDH-loss strains appear to grow only by fermentation. Statistical analysis of growth at 24 h is shown in Fig. 2C. Similar overall levels of growth in AS media are observed, as expected. In contrast, growth in ISE minimal galactose media reveals large differences in fitness, also as expected (Smith *et al.* 2007). Compared to growth in AS, WT growth in ISE is most robust, with *sdh1Δ* and *sdh2Δ* showing impaired growth, and the *jlp1Δ* strain strongly disabled for growth in ISE media (Fig. 2B), as previously reported (Smith

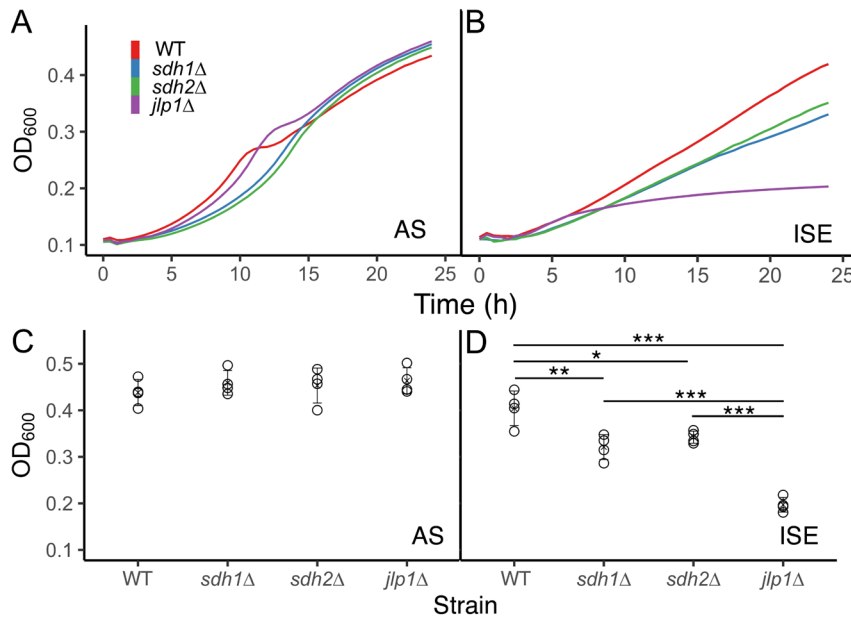


Figure 2 Representative yeast growth phenotypes. (A) Growth in ammonium sulfate medium. (B) Growth in ISE medium. (C) Growth in ammonium sulfate medium at 24 h. (D) Growth in ISE medium at 24 h. Statistical significance reflecting four replicates is reported using a one-way ANOVA with a *post hoc* Tukey HSD test for significance. *P*-values: * < 0.05, ** < 0.01, *** < 0.001.

et al. 2007). These growth differences were statistically significant except that the growth of the SDH-loss strains was indistinguishable (Fig. 2D). We interpret the growth defect of SDH-loss yeast strains in ISE medium as evidence

that Jlp1p dioxygenase function is compromised in these strains, either due to succinate inhibition or oxidative stress affecting the required ferrous ion. These data confirm the findings of Smith *et al.* and lay the basis for screening

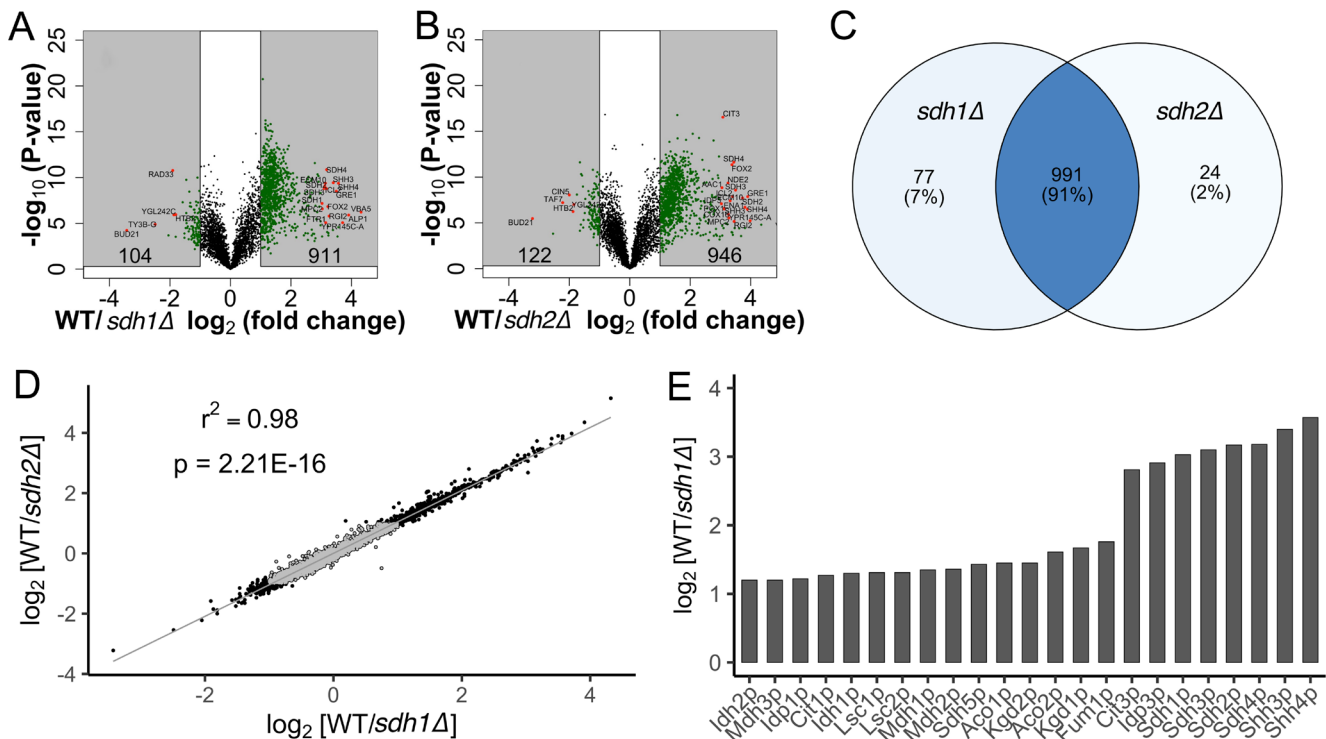


Figure 3 Proteomic comparison of *sdh1*Δ and *sdh2*Δ yeast strains. (A and B) Volcano plots. Shading denotes significance ($P < 0.05$ and $|\log_2(\text{fold-change})| > 1.5$). Protein counts in each category are indicated. (C) Venn diagram indicating relationship between proteins significantly different from WT for *sdh1*Δ and *sdh2*Δ cells. (D) Correlation between *sdh1*Δ and *sdh2*Δ proteome alterations. Gray points indicate genes with non-significant fold changes. (E) Results of DAVID functional analysis indicating loss of TCA cycle enzyme polypeptides, especially SDH subunits, in *sdh1*Δ yeast.

for compounds that suppress the *sdh1Δ* and *sdh2Δ* growth defect in ISE media.

Proteomic analysis

Previous data indicated that both *sdh1Δ* and *sdh2Δ* strains lack SDH activity but that some Sdh1p protein could be detected in *sdh2Δ* yeast (Smith *et al.* 2007). In preparation for the chemical suppression screen to identify compounds that rescue Jlp1p activity, we studied potential subtle differences between *sdh1Δ* and *sdh2Δ* strains to select one for screening. We therefore performed a detailed proteomic analysis of WT, *sdh1Δ*, and *sdh2Δ* yeast strains. Mitochondria were isolated from replicate strains grown in YP-rich media containing galactose. Extracted proteins were digested with trypsin and peptide lysines acylated using isobaric tags, and the resulting samples were analyzed by LC-MS. Approximately, 6000 proteins were detected, indicating that even the purified mitochondrial fractions contain a representation of much of the yeast proteome. Quantitative analyses compared detected proteins between WT/*sdh1Δ*, WT/*sdh2Δ*, and *sdh1Δ/sdh2Δ* and reported as log₂(fold-change) with statistical significance as an adjusted *P*-value (significance < 0.05).

Volcano plots (Fig. 3A and B) indicate differences between WT and SDH-loss strains. In the WT/*sdh1Δ* dataset, 1015 proteins were significantly different between WT and *sdh1Δ* yeast, with 911 more abundant in WT and 104 more abundant in *sdh1Δ*. In the WT/*sdh2Δ* dataset, 1068 proteins were significantly different between WT and *sdh1Δ* yeast, with 946 more abundant in WT and 122 more abundant in *sdh1Δ*. These results confirm the large remodeling of the yeast proteome driven by SDH loss. Data for the most altered proteins are found in Supplementary Table 3. Many of the highlighted proteins are from central metabolic pathways, including TCA cycle proteins (SDH, Cit3p, Idp3p). Other TCA cycle proteins are among those with significantly reduced expression in SDH-loss yeast, suggesting a general loss of mitochondrial oxidative phosphorylation functions, as expected. Other important mitochondrial proteins, such as those from the electron transport chain, were significantly reduced in SDH-loss yeast (Nde2p, Cox16p, Cyb2p). Some other proteins higher in WT than SDH-loss cells are peripherally related to respiratory metabolism, including mitochondrial pyruvate transporters (Mpc2p) and respiratory growth-induced protein 2 (Rgi2p). Additionally, Ftr1p, the yeast cell surface iron importer, is greatly reduced in SDH-loss cells. This indicates that iron uptake and regulation are dysregulated upon SDH-loss, consistent with mammalian cell models (Goncalves *et al.* 2021). In

contrast, the few proteins that are significantly increased upon SDH loss yeast are more difficult to rationalize. These include histone H2B (Htb2p), Bud21p, a protein involved in transcription regulation and several other proteins related to gene transcription and regulation (Taf7p, Rad33p, Ty3B-Gp, and Cin5p). Overall, proteins reduced upon SDH loss include mitochondrial proteins, enzymes of aerobic respiration, and iron import factors. Because SDH plays a key role in both the TCA cycle and electron transport chain, it is reasonable that proteins representing both the TCA cycle and electron transport chain are impacted by SDH loss. Despite these changes to mitochondrial physiology, levels of glycolytic enzymes were not significantly changed upon SDH loss. Thus, hexokinase, phosphofructokinase, and pyruvate kinase all experienced changes between 0.8- and 1.2-fold upon SDH loss.

We compared the SDH-loss strains in greater detail. Of the 1092 proteins that were differentially expressed upon SDH loss, 991 of these (91%) were shared between both *sdh1Δ* and *sdh2Δ*, 77 (7%) were unique to the WT/*sdh1Δ* dataset, and 24 (2%) were unique to the WT/*sdh2Δ* dataset (Fig. 3C). This analysis confirms that *sdh1Δ* and *sdh2Δ* are proteomically comparable and this is affirmed by a correlation plot (Fig. 3D).

Applying pathway analysis using the DAVID Functional Annotation Tool (DAVID Bioinformatics Resources 6.8, NIAID/NIH), we found, as expected, that major proteomic changes in SDH-loss cells focused on enzymes of the TCA cycle. Quantitation of these enzyme changes is shown in (Fig. 3E). In this case, ratios are rough estimates due to peptide counting methods, such that complete absence of Sdh1p in *sdh1Δ* compared to WT yields a nominal ~10-fold change. Interestingly, loss of Sdh1p reduced most TCA cycle enzymes by 2- to 3-fold but reduced SDH subunits (including Shh3p and Shh4p) to a greater extent.

The current proteomic data also allowed verification of the prior finding that both Sdh1p and Sdh2p are lost in *sdh1Δ* yeast, but a fraction of Sdh1p remains detectable in *sdh2Δ* yeast (Smith *et al.* 2007). Such evidence is shown in Supplementary Fig. 4. This result is reminiscent of reports from mammalian cells where a complex of the SDHA catalytic subunit and chaperones appears to persist in the absence of SDHB (Bezawork-Geleta *et al.* 2018). Though there is no evidence of enzyme activity for the residual catalytic subunit, it might contribute in subtle ways to the different phenotypes of tumors driven by loss of different SDH subunits (Guzy *et al.* 2008). Thus, the small proteomic differences between *sdh1Δ* and *sdh2Δ* yeast may serve as a paradigm for small but important differences in comparable mammalian mutants affecting different SDH subunits.

For example, the yeast Sdh3p subunit also functions as a component of the TIM22 mitochondrial translocase system, and yeast also express Shh3p and Shh4p paralogs of Sdh3p and Sdh4p but with unknown functions (Gebert *et al.* 2011). The overall strong phenotypic and proteomic similarity of *sdh1Δ* and *sdh2Δ* strains led us to select the *sdh1Δ* strain as representative and appropriate for chemical suppression screening.

LOPAC suppression screen

High-throughput screening is an essential approach in drug discovery research (Macarron *et al.* 2011). We previously conducted a lethality screen of more than 200,000 compounds seeking agents selectively toxic to SDH-loss yeast cells as models of SDH-loss human familial PGL (Bancos *et al.* 2013). The current suppression screen focuses on the concept that the fundamental pathologies of SDH-loss cells are driven by the accumulation of succinate as an oncometabolite inhibiting 2-ketoglutarate-dependent dioxygenases (Koivunen *et al.* 2007, Cervera *et al.* 2009, Xiao *et al.* 2012, Letouzé *et al.* 2013). We

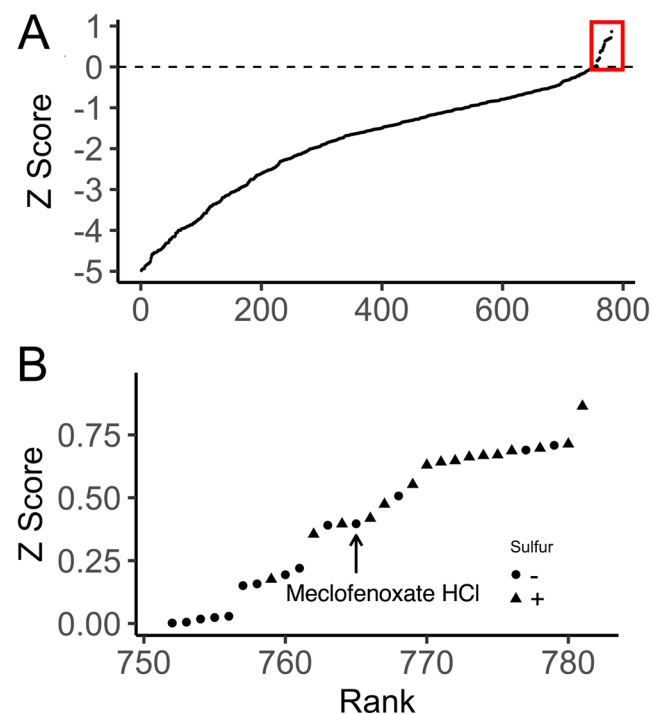


Figure 4
Results of LOPAC chemical suppression screen. (A) Effects of LOPAC compounds on *sdh1Δ* yeast growth in ISE medium, ranked for compounds with Z Scores > -5. Red box at upper right indicates compounds with Z > 0. (B) Detail of LOPAC compounds inducing Z Scores > 0, indicating whether the compound formulation itself did (+) or did not (-) contain bioavailable sulfate. Arrow indicates meclofenoxate HCl (Z = 0.40).

hypothesized that ameliorating succinate toxicity may normalize cell function. Beyond succinate intoxication, it has been proposed that ROS also accumulate in SDH-loss cells, potentially compromising dioxygenase function by oxidation of the ferrous ion critical to dioxygenase function (Liu *et al.* 2020). The present suppression screen therefore was developed to identify compounds that selectively rescue the growth of *sdh1Δ* yeast by restoring Jlp1p function using growth in ISE as the selection.

The LOPAC₁₂₈₀ library (Sigma-Aldrich) was screened at 10 μM in 16 96-well plates with 80 compounds per plate, allowing for growth controls (WT and *sdh1Δ* strains in AS and ISE media). Each experimental well was seeded with *sdh1Δ* yeast in ISE media and OD₆₀₀ readings were taken at seven timepoints over a 24-h period and a score modeled on the conventional Z statistic was calculated for each treatment and time (Materials and methods). Compounds characterized by Z > 0 for at least 6 of 7 timepoints were classified as hits (30 of 1280 compounds; Fig. 4A).

Hit validation

Because the suppression screen was based on sulfur scavenging, drugs formulated with sulfate or related compounds (16/30 hits) were either excluded or more

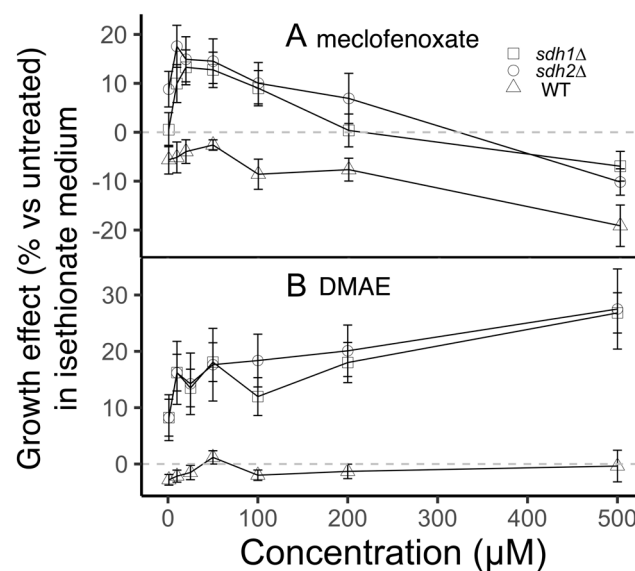
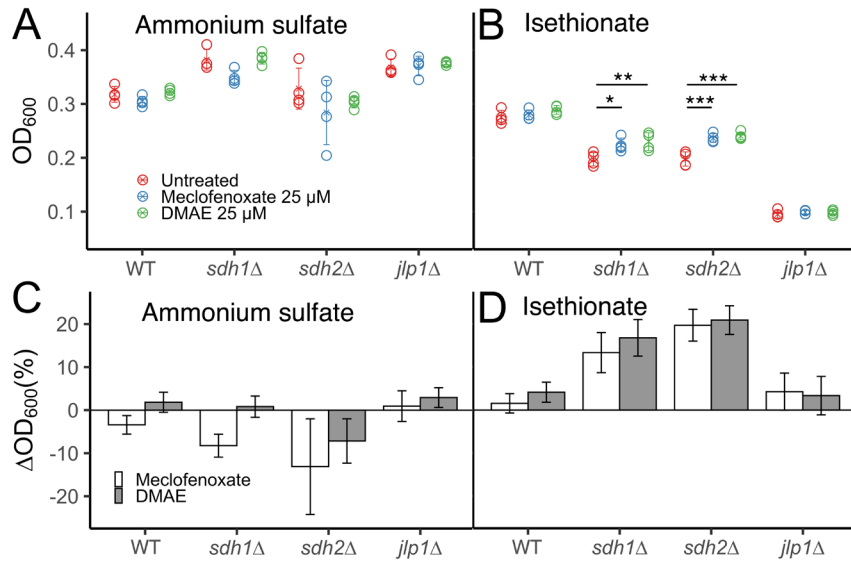


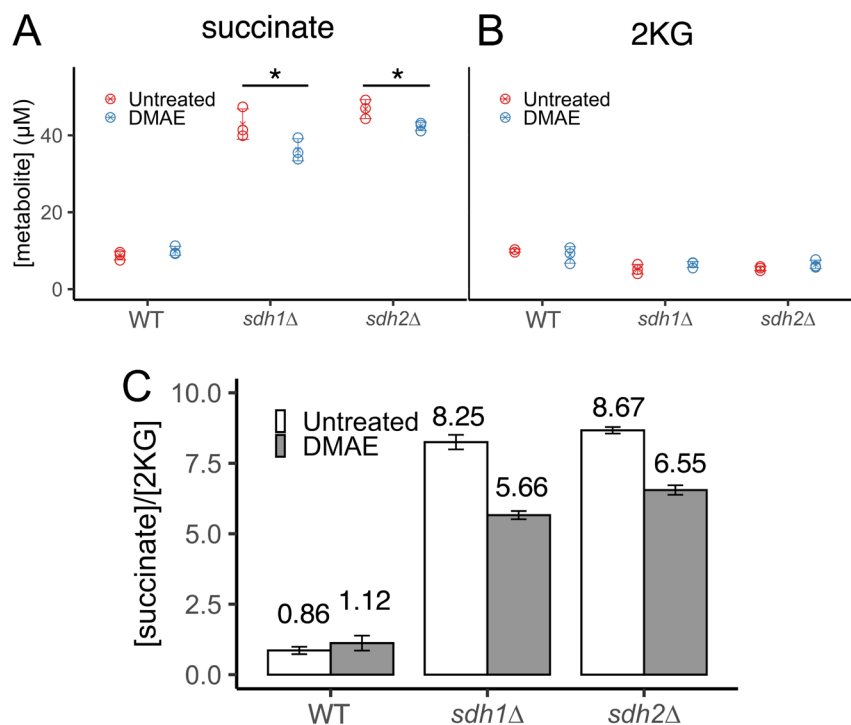
Figure 5
Dose-response data (percent change relative to untreated) for the indicated yeast strains in ISE medium and the indicated concentrations of (A) meclofenoxate and (B) DMAE, both dissolved in water. For statistical analysis, normalization was performed by converting OD₆₀₀ readings to percent growth change (treated cells vs control cells). The s.e. of the four technical replicates was also propagated from an OD₆₀₀ error to a percentage growth change error and plotted as error bars.

**Figure 6**

Effect of 25 µM treatment of the indicated drugs on yeast growth at 24 h in (A) AS and (B) ISE media. Drug effects are shown as % growth change in (C) AS and (D) ISE media for the indicated drug treatments. Statistical significance is reported using two-way ANOVA with a *post hoc* Tukey HSD test for significance. *P*-values: * < 0.05, ** < 0.01, *** < 0.001. In panel B, error bars indicate s.d. of four technical replicates propagated to % growth effect vs untreated.

rigorously tested (Fig. 4B). Four of the initial 30 hits formed colored solutions that interfered with OD₆₀₀ readings so were excluded. Seven compounds with highest Z-scores not attributable to sulfur content or formulation (phenanthroline, phentolamine, reserpine, protoporphyrin IX, minocycline, pyrrolidinedithiocarbamate, and meclofenoxate) were repurchased and subjected to further validation (Supplementary Fig. 2). Some of these top hits had been deemed intriguing because of reported metal chelating properties. Validation assays were performed in 96-well

plates grown without shaking. Oxygenation was judged adequate by the observation that the oxygen-dependent Jlp1p dioxygenase in WT cells allowed strong growth in minimal ISE galactose media. Validation screening compared concentration-dependent effects of test compounds on the growth of WT, *sdh1*Δ, *sdh2*Δ and *jlp1*Δ strains on both ISE and AS media, seeking compounds that selectively improved growth only of *sdh1*Δ and *sdh2*Δ strains and only on ISE media. A summary of the findings of follow-up validation studies is presented in Supplementary Table 2.

**Figure 7**

Effect of 100 µM DMAE on (A) intracellular succinate and (B) intracellular 2KG concentrations in ISE medium after 24 h. Indicated level of statistical significance from a two-way ANOVA with a *post hoc* Tukey HSD test for significance. **P* < 0.05 based on three replicates. (C) Ratio of succinate concentration to 2KG concentration in samples. Error bars represent s.d. for three replicates.

This procedure led to the identification of meclufenoxate HCl (Goldman & Klatz 2003) as the most robust and reproducible hit (Fig. 5A). Meclofenoxate is an ester reported to rapidly hydrolyze in water to its substituents, DMAE and 4-chlorophenoxyacetic acid (Supplementary Fig. 3; (Yoshioka *et al.* 1987)). Testing of these substituents showed DMAE to be the active agent (Fig. 5B and Supplementary Fig. 4). Meclofenoxate HCl and DMAE (25 μ M) were then validated in a full comparative growth assay (Fig. 6), demonstrating their ability to selectively suppress the growth defect of SDH-loss yeast on minimal galactose medium with ISE as sulfur source. Selective partial suppression of the growth defect of SDH-loss yeast in ISE medium, without growth stimulation of WT or *jlp1 Δ* strains in ISE media, or any of the strains in AS media, suggests that meclufenoxate HCl and DMAE act by improving Jlp1p catalysis of ISE conversion to sulfite. We sought evidence for potential mechanisms of this effect.

Metabolomics

Meclofenoxate HCl and DMAE have been studied as anti-aging treatments in animals and in assays of improved brain

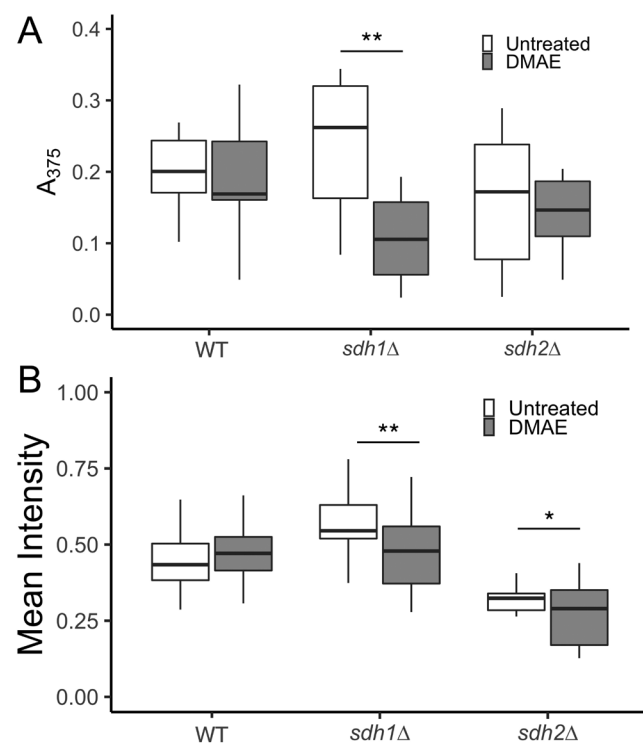


Figure 8
Effect of 100 μ M DMAE treatment on measures of oxidative stress in ISE medium after 24 h. (A) Assay of protein carbonyl products. (B) Assay of ROS in live cells. Indicated level of statistical significance from a two-way ANOVA with a *post hoc* Tukey HSD test for significance. * $P < 0.05$ and ** $P < 0.01$ based on 12 replicates (A) and 30–60 cells (B).

function (Goldenberg 1969, Miyazaki *et al.* 1976, Marcer & Hopkins 1977, Zuckerman & Barrett 1978, Dowson 1985, Petkov *et al.* 1990, Kovalev *et al.* 2008) but with little mechanistic detail. There is early published evidence that DMAE activates certain enzymes, including glucose-6-phosphate dehydrogenase (Bielenberg *et al.* 1986). We used NMR metabolomics to quantify key identifiable metabolites in WT, *sdh1 Δ* , and *sdh2 Δ* yeast with and without treatment with 100 μ M DMAE. The primary goal was to monitor intracellular levels of succinate and 2KG, the metabolites whose concentration ratio is thought to determine dioxygenase inhibition (Fig. 7A and B). Other metabolites were detected and quantitated, including TCA metabolites, pyrimidine biosynthesis intermediates, and amino acids. We profiled a total of 46 metabolites, 43 with accurate concentrations from the Chenomx database, and 3 with relative concentrations from the Human Metabolome Database. Concentrations and s.d. (from three replicates) for all metabolites are provided in Supplementary Table 4.

Metabolic profiling of WT, *sdh1 Δ* , and *sdh2 Δ* yeast follows known effects of SDH loss on eukaryotic cells. Succinate accumulated up to five-fold higher in *sdh1 Δ* and *sdh2 Δ* than in WT cells. Amino acids such as glycine, leucine, phenylalanine, and tryptophan also accumulate in SDH-loss cells, while there was a reduction in levels of thiamine, uridine, pyruvate, glycerol, glutamate, and notably, 2-ketoglutarate. Other metabolites showed smaller, but significant, differences.

Remarkably, DMAE treatment significantly reduced intracellular succinate concentrations in both *sdh1 Δ* and *sdh2 Δ* yeast strains but not in WT yeast. Because the succinate/2KG ratio determines dioxygenase function, this partial normalization of the ratio (Fig. 7C) suggests the basis for meclufenoxate as a hit on this screen. Besides succinate reduction, DMAE has other interesting effects on SDH-loss yeast metabolites. As a choline precursor, DMAE increases choline by eight- to nine-fold in treated strains. A downstream metabolite, *sn*-glycero-3-phosphocholine, was also increased in SDH-loss strains treated by DMAE. Valine and leucine amino acid degradation pathways appear to be enhanced by DMAE, with both amino acids showing lower abundance in DMAE-treated SDH-loss strains, while their downstream compound, 3-isopropylmalate, is increased. Other notable DMAE-induced changes are reductions in tryptophan, phenylalanine, and ornithine, as well as increases in nucleotide-related compounds thiamine and orotidine. Higher levels of orotidine imply a diversion of carbon from glycolysis to the pentose phosphate pathway (PPP) and pyrimidine biosynthesis, but we detect no obvious shunting of carbon from the TCA cycle (pyruvate

and citrate levels are not changed). A simple rationale for DMAE-induced succinate reduction is thus elusive.

ROS assays

Though succinate toxicity is thought to be the primary oncometabolite in SDH-loss PGL, evidence shows that ROS may also accumulate and contribute to the development of a cancer phenotype (Ishii *et al.* 2005, Smith *et al.* 2007). An altered intracellular redox state has the potential to shift the Fe²⁺: Fe³⁺ balance required for cycles of dioxygenase activity (Guzy *et al.* 2008, Liu *et al.* 2020). SDH-loss yeast have been shown to suffer increased ROS production with some increase in the formation of protein carbonyl damage (Weber *et al.* 2015) but no acute evidence of toxic DNA damage (Smith *et al.* 2007). Assays monitoring the effects of DMAE treatment on protein oxidative damage yielded mixed results (Fig. 8A). DMAE treatment significantly reduced protein carbonyl levels in *sdh1Δ* cells but not in *sdh2Δ* or WT cells.

To more directly monitor ROS production, live cells were imaged via fluorescence microscopy after treatment with a fluorescein derivative activated by ROS. Results are shown in Fig. 8B, and example images are shown in Supplementary Fig. 5. Both *sdh1Δ* and *sdh2Δ* show significant decreases in fluorescence after treatment with DMAE, while WT showed no effect. Interestingly, untreated *sdh2Δ* cells demonstrated a lower mean fluorescence intensity than untreated WT cells, different from earlier findings that ROS production was similarly increased in both *sdh1Δ* and *sdh2Δ* yeast (Smith *et al.* 2007). Replicative experiments were performed with DHE staining. DMAE exhibited similarly subtle anti-oxidant activity (Supplementary Fig. 6). These results suggest that anti-oxidant effects could also play a role in DMAE suppression of Jlp1p inhibition. Previous studies of such effects for DMAE have been limited to much higher concentrations (Malanga *et al.* 2012).

Implications

The disease consequences of metabolic perturbation are of central importance in medicine. Metabolic changes in cancer have been detected and discussed since the discovery of the Warburg effect (Warburg 1956, Pavlova & Thompson 2016, de Alteriis *et al.* 2018, Kozal *et al.* 2021). SDH-loss familial PGL presents a unique metabolic state with its fragmented TCA cycle. The highly conserved nature of SDH across evolution makes our detailed proteomic comparison of *sdh1Δ* and *sdh2Δ* strains particularly interesting and relevant for understanding the long-standing paradox that,

contrary to expectation for a multi-subunit enzyme, SDH-loss tumors show phenotypes dependent on the affected SDH subunit (Neumann *et al.* 2004, Guzy *et al.* 2008, Andrews *et al.* 2018, Rijken *et al.* 2019). While loss of any SDH subunit might be predicted to be equally disturbing to cell metabolism, there is evidence from human familial PGL that this is not true. By analogy with the mammalian case where residual SDH complexes may differ upon loss of certain subunits (Bezawork-Geleta *et al.* 2018), it is intriguing that SDH-loss yeast lacking Sdh1p show subtle proteomic differences from strains lacking Sdh2p. Rather than stressing the similarities between *sdh1Δ* and *sdh2Δ* for the purposes of our yeast screen, the subtle differences between the two strains may illuminate the differential penetrance of PGL caused by SDHA loss vs SDHB loss in humans. There are ~20 differentially expressed proteins between *sdh1Δ* and *sdh2Δ* yeast strains and two interesting cases are Cox19p and Cox16p, both assembly factors for cytochrome c oxidase. These proteins are less abundant in the *sdh2Δ* strain than *sdh1Δ* strain, giving us a clue as to subtle proteomic differences that might have larger differences on disease progression among different human SDH-loss PGLs.

Research in familial PGL has focused primarily on three potential oncogenic mechanisms upon SDH loss: succinate accumulation driving dioxygenase inhibition (Selak *et al.* 2005, Koivunen *et al.* 2007, Smith *et al.* 2007, Xiao *et al.* 2012), ROS overproduction with corresponding damage and redox imbalance (Ishii *et al.* 2005, Saffi *et al.* 2006, Kregiel 2012, Her & Maher 2015, Liu *et al.* 2020), and succinylation of proteins leading to dysfunction (Smestad *et al.* 2017, 2018). It is becoming more apparent that all of these mechanisms play a role in oncogenesis through analysis of recently developed cell lines model. By comparing SdhB and SdhD loss mouse chromaffin cells that model adrenal PGL, researchers have shown how the residual SDH left by SdhB loss contributes to a more aggressive phenotype than SdhD loss by triggering iron imbalance and ROS generation (Goncalves *et al.* 2021). Using the linkage between SDH loss and dioxygenase inhibition as a paradigm, the present chemical suppression screen exploited our ability to connect the inhibition of sulfur scavenging dioxygenase Jlp1p to a nutritional growth assay in a sulfur source requiring Jlp1p function in *S. cerevisiae* (Hogan *et al.* 1999, Smith *et al.* 2007). The leading hit from this screen, meclufenoxate HCl, and its active derivative DMAE, selectively increase the growth of SDH-loss yeast strains by 10–20% in ISE media. Considering the role played by iron in modulating dioxygenase activity in mammalian cells, an analogs screen might be envisioned that focuses on the restoration of mammalian iron homeostasis rather than fungal sulfur metabolism. Because iron drives the epithelial–

mesenchymal transition in mammalian cells, compounds that increase iron availability might restore dioxygenase function in cells where it is inhibited by excess succinate (Müller *et al.* 2020).

Though studied superficially over many years, potential mechanisms of meclofenoxate and DMAE effects on metabolism, physiology, and lifespan remain poorly understood. Initial studies in the 1970s suggested that these drugs substantially enhance the lifespan of mice (Hochschild 1973, Miyazaki *et al.* 1976). DMAE was found to affect brain tissue, reducing levels of lipofuscin, an oxidative plaque associated with aging. Lohr and Acara noted that DMAE is similar in structure to choline and could potentially serve as a precursor and that it could also inhibit choline oxidase (Lohr & Acara 1990), reducing levels of betaine. Anti-aging effects of DMAE have been studied with an eye to a potential free-radical scavenging mechanism (Malanga *et al.* 2012).

Perhaps the most tantalizing published mechanistic observation for DMAE is its reported ability to increase the activity of glucose-6-phosphate dehydrogenase, the rate-limiting initial enzyme of the PPP (Roy & Singh 1983). The PPP runs parallel to glycolysis but generates reducing equivalents and key carbon skeletons for nucleotide biosynthesis without generating ATP. We hypothesize that agents such as DMAE may enhance dioxygenase function in SDH-loss cells by shunting carbon flux away from glycolysis and the TCA cycle, reducing the production of succinate at the SDH blockade. We find minor indications of increased flux through the PPP resulting from DMAE treatment, though the metabolic origin of succinate decrease remains unclear. We provide further evidence that DMAE relieves oxidative stress by reducing ROS, perhaps normalizing the obligatory $\text{Fe}^{2+}:\text{Fe}^{3+}$ equilibrium essential to the dioxygenase catalytic cycle.

Thus, this work illustrates a new paradigm for rewiring metabolism through a small molecule cue that reduces oncometabolite accumulation. Searching for effective small molecules of this type that might affect SDH-loss PGL tumor cells offers a potential route to normalizing inhibited dioxygenase function in such cells. Because dioxygenase inhibition by succinate causes both pseudohypoxia and histone and DNA hypermethylation, such metabolic rewiring could have broad therapeutic effects in familial PGL.

Supplementary materials

This is linked to the online version of the paper at <https://doi.org/10.1530/ERC-21-0349>.

Declaration of interest

The authors declare that there is no conflict of interest that could be perceived as prejudicing the impartiality of the research reported.

Funding

This work was supported by the Mayo Foundation, the Mayo Clinic Graduate School of Biomedical Sciences, and the Paradifference Foundation.

Author contribution statement

Project conception and manuscript preparation: W B, M B, L J M; Experiments: W B, M B, K S, K P, B W; Data analysis: W B, M B, K S, K P, B W.

Acknowledgements

The authors thank members of the Maher laboratory for assistance and Marina Ramirez-Alvarado for sharing instrumentation. The authors acknowledge the excellent assistance of members of the Katzmann laboratory at Mayo Clinic, especially Chun Che Tseng. The excellent support of Ivan Vuckovic and Song Zhang in the Mayo Clinic NMR core facility, Akhilesh Pandey, Zachary Ryan, and Benjamin Madden in the Mayo Clinic Proteomics core facility, and Mai Petterson and Ian Lanza in the Mayo Clinic Metabolomics core facility are acknowledged.

References

- Goldman R & Klatz R 2003 *The Science of Anti-Aging Medicine*. Boca Raton, FL, USA: American Academy of Anti-Aging Medicine.
- Adachi H, Fujiwara Y & Ishii N 1998 Effects of oxygen on protein carbonyl and aging in *Caenorhabditis elegans* mutants with long (age-1) and short (mev-1) life spans. *Journals of Gerontology: Series A, Biological Sciences and Medical Sciences* **53** B240–B244. (<https://doi.org/10.1093/gerona/53a.4.b240>)
- Andrews KA, Ascher DB, Pires DEV, Barnes DR, Vialard L, Casey RT, Bradshaw N, Adlard J, Aylwin S, Brennan P, *et al.* 2018 Tumour risks and genotype–phenotype correlations associated with germline variants in succinate dehydrogenase subunit genes SDHB, SDHC and SDHD. *Journal of Medical Genetics* **55** 384–394. (<https://doi.org/10.1136/jmedgenet-2017-105127>)
- Astuti D, Latif F, Dallol A, Dahia PLM, Douglas F, George E, Sköldbberg F, Husebye ES, Eng C & Maher ER 2001 Gene mutations in the succinate dehydrogenase subunit SDHB cause susceptibility to familial pheochromocytoma and to familial paraganglioma. *American Journal of Human Genetics* **69** 49–54. (<https://doi.org/10.1086/321282>)
- Bancos I, Bida JP, Tian D, Bundrick M, John K, Holte MN, Her YF, Evans D, Saenz DT, Poeschla EM, *et al.* 2013 High-throughput screening for growth inhibitors using a yeast model of familial paraganglioma. *PLoS ONE* **8** e56827. (<https://doi.org/10.1371/journal.pone.0056827>)
- Baysal BE, Ferrell RE, Willett-Brozick JE, Lawrence EC, Myssiorek D, Bosch A, Mey A van der, Taschner PEM, Rubinstein WS, Myers EN, *et al.* 2000 Mutations in SDHD, a mitochondrial complex II gene, in hereditary paraganglioma. *Science* **287** 848–851. (<https://doi.org/10.1126/science.287.5454.848>)
- Berends AMA, Buitenwerf E, de Krijger RR, Veeger NJGM, van der Horst-Schrivers ANA, Links TP & Kerstens MN 2018 Incidence of pheochromocytoma and sympathetic paraganglioma in the Netherlands: a nationwide study and systematic review. *European Journal of Internal Medicine* **51** 68–73. (<https://doi.org/10.1016/j.ejim.2018.01.015>)
- Bezawork-Geleta A, Wen H, Dong L, Yan B, Vider J, Boukalova S, Krobava L, Vanova K, Zobalova R, Sobol M, *et al.* 2018 Alternative assembly of respiratory complex II connects energy stress to metabolic checkpoints. *Nature Communications* **9** 2221. (<https://doi.org/10.1038/s41467-018-04603-z>)
- Bielenberg GW, Hayn C & Kriegstein J 1986 Effects of cerebro-protective agents on enzyme activities of rat primary glial cultures and rat cerebral cortex. *Biochemical Pharmacology* **35** 2693–2702. ([https://doi.org/10.1016/0006-2952\(86\)90177-2](https://doi.org/10.1016/0006-2952(86)90177-2))

- Braun MM, Damjanac T, Zhang Y, Chen C, Hu J & Maher LJ 2019 Modeling succinate dehydrogenase loss disorders in *C. elegans* through effects on hypoxia-inducible factor. *PLoS ONE* **14** e0227033. (<https://doi.org/10.1371/journal.pone.0227033>)
- Burnichon N, Brière JJ, Libé R, Vescovo L, Rivière J, Tissier F, Jouanno E, Jeunemaitre X, Bénit P, Tzagoloff A, *et al.* 2010 SDHA is a tumor suppressor gene causing paraganglioma. *Human Molecular Genetics* **19** 3011–3020. (<https://doi.org/10.1093/hmg/ddq206>)
- Cervera AM, Bayley JP, Devilee P & McCreath KJ 2009 Inhibition of succinate dehydrogenase dysregulates histone modification in mammalian cells. *Molecular Cancer* **8** 89. (<https://doi.org/10.1186/1476-4598-8-89>)
- Cherest H & Surdin-Kerjan Y 1992 Genetic analysis of a new mutation conferring cysteine auxotrophy in *Saccharomyces cerevisiae*: updating of the sulfur metabolism pathway. *Genetics* **130** 51–58. (<https://doi.org/10.1093/genetics/130.1.51>)
- de Alteriis E, Carteni F, Parascandola P, Serpa J & Mazzoleni S 2018 Revisiting the Crabtree/Warburg effect in a dynamic perspective: a fitness advantage against sugar-induced cell death. *Cell Cycle* **17** 688–701. (<https://doi.org/10.1080/15384101.2018.1442622>)
- Dona M, Waaijers S, Richter S, Eisenhofer G, Korving J, Kamel SM, Bakkers J, Rapizzi E, Rodenburg RJ, Zethof J, *et al.* 2021 Loss of *sdhb* in zebrafish larvae recapitulates human paraganglioma characteristics. *Endocrine-Related Cancer* **28** 65–77. (<https://doi.org/10.1530/ERC-20-0308>)
- Dowson JH 1985 Quantitative studies of the effects of aging, meclufenoxate, and dihydroergotamine on intraneuronal lipopigment accumulation in the rat. *Experimental Gerontology* **20** 333–340. ([https://doi.org/10.1016/0531-5565\(85\)90013-0](https://doi.org/10.1016/0531-5565(85)90013-0))
- Erickson D, Kudva YC, Ebersold MJ, Thompson GB, Grant CS, van Heerden JA & Young Jr WF 2001 Benign paragangliomas: clinical presentation and treatment outcomes in 236 patients. *Journal of Clinical Endocrinology and Metabolism* **86** 5210–5216. (<https://doi.org/10.1210/jcem.86.11.8034>)
- Feyder S, De Craene JO, Bär S, Bertazzi DL & Friant S 2015 Membrane trafficking in the yeast *Saccharomyces cerevisiae* model. *International Journal of Molecular Sciences* **16** 1509–1525. (<https://doi.org/10.3390/ijms16011509>)
- Gebert N, Gebert M, Oeljeklaus S, von der Malsburg K, Stroud DA, Kulawiak B, Wirth C, Zahedi RP, Dolezal P, Wiese S, *et al.* 2011 Dual function of Sdh3 in the respiratory chain and TIM22 protein translocase of the mitochondrial inner membrane. *Molecular Cell* **44** 811–818. (<https://doi.org/10.1016/j.molcel.2011.09.025>)
- Gerald D, Berra E, Frapart YM, Chan DA, Giaccia AJ, Mansuy D, Pouyssegur J, Yaniv M & Mechta-Grigoriou F 2004 JunD reduces tumor angiogenesis by protecting cells from oxidative stress. *Cell* **118** 781–794. (<https://doi.org/10.1016/j.cell.2004.08.025>)
- Goffeau A, Barrell BG, Bussey H, Davis RW, Dujon B, Feldmann H, Galibert F, Hoheisel JD, Jacq C, Johnston M, *et al.* 1996 Life with 6000 genes. *Science* **274** 546, 563–567. (<https://doi.org/10.1126/science.274.5287.546>)
- Goldenberg MM 1969 Effect of atropine and DMAE (a hemicholinium derivative) on contractile responses of the guinea pig ileum. *Canadian Journal of Physiology and Pharmacology* **47** 185–192. (<https://doi.org/10.1139/y69-032>)
- Goncalves J, Moog S, Morin A, Gentric G, Müller S, Morrell AP, Kluckova K, Stewart TJ, Andoniadou CL, Lussey-Lepoutre C, *et al.* 2021 Loss of SDHB promotes dysregulated iron homeostasis, oxidative stress, and sensitivity to ascorbate. *Cancer Research* **81** 3480–3494. (<https://doi.org/10.1158/0008-5472.CAN-20-2936>)
- Gregg C, Kyryakov P & Titorenko VI 2009 Purification of mitochondria from yeast cells. *Journal of Visualized Experiments* **30** 1417. (<https://doi.org/10.3791/1417>)
- Guzy RD, Sharma B, Bell E, Chandel NS & Schumacker PT 2008 Loss of the SdhB, but not the SdhA, subunit of complex II triggers reactive oxygen species-dependent hypoxia-inducible factor activation and tumorigenesis. *Molecular and Cellular Biology* **28** 718–731. (<https://doi.org/10.1128/MCB.01338-07>)
- Hao HX, Khalimonchuk O, Schraders M, Dephore N, Bayley JP, Kunst H, Devilee P, Cremers CWRJ, Schiffman JD, Bentz BG, *et al.* 2009 SDHS, a gene required for flavination of succinate dehydrogenase, is mutated in paraganglioma. *Science* **325** 1139–1142. (<https://doi.org/10.1126/science.1175689>)
- Her YF & Maher LJ 2015 Succinate dehydrogenase loss in familial paraganglioma: biochemistry, genetics, and epigenetics. *International Journal of Endocrinology* **2015** 296167. (<https://doi.org/10.1155/2015/296167>)
- Hochschild R 1973 Effect of dimethylaminoethyl p-chlorophenoxyacetate on the life span of male Swiss Webster albino mice. *Experimental Gerontology* **8** 177–183. ([https://doi.org/10.1016/0531-5565\(73\)90024-7](https://doi.org/10.1016/0531-5565(73)90024-7))
- Hogan DA, Auchtung TA & Hausinger RP 1999 Cloning and characterization of a sulfonate/α-ketoglutarate dioxygenase from *Saccharomyces cerevisiae*. *Journal of Bacteriology* **181** 5876–5879. (<https://doi.org/10.1128/JB.181.18.5876-5879.1999>)
- Hung CW, Martínez-Márquez JY, Javed FT & Duncan MC 2018 A simple and inexpensive quantitative technique for determining chemical sensitivity in *Saccharomyces cerevisiae*. *Scientific Reports* **8** 11919. (<https://doi.org/10.1038/s41598-018-30305-z>)
- Ishii T, Yasuda K, Akatsuka A, Hino O, Hartman PS & Ishii N 2005 A mutation in the SDHC gene of complex II increases oxidative stress, resulting in apoptosis and tumorigenesis. *Cancer Research* **65** 203–209.
- Kayikci Ö & Nielsen J 2015 Glucose repression in *Saccharomyces cerevisiae*. *FEMS Yeast Research* **15** fov068. (<https://doi.org/10.1093/femsyr/fov068>)
- Klučková K, Thakker A, Vettore L, Escribano-Gonzalez C, Hindshaw RL, Tearle JLE, Goncalves J, Kaul B, Lavery GG, Favier J, *et al.* 2020 Succinate dehydrogenase deficiency in a chromaffin cell model retains metabolic fitness through the maintenance of mitochondrial NADH oxidoreductase function. *FASEB Journal* **34** 303–315. (<https://doi.org/10.1096/fj.201901456R>)
- Koivunen P, Hirsilä M, Remes AM, Hassinen IE, Kivirikko KI & Myllyharju J 2007 Inhibition of hypoxia-inducible factor (HIF) hydroxylases by citric acid cycle intermediates: possible links between cell metabolism and stabilization of HIF. *Journal of Biological Chemistry* **282** 4524–4532. (<https://doi.org/10.1074/jbc.M610415200>)
- Kovalev GI, Firstova Iulu & Salimov RM 2008 Effects of piracetam and meclufenoxate on the brain NMDA and nicotinic receptors in mice with different exploratory efficacy in the cross maze test. *Eksperimental'Naia i Klinicheskaia Farmakologija* **71** 12–17.
- Kozal K, Jóźwiak P & Krześlak A 2021 Contemporary perspectives on the Warburg effect inhibition in cancer therapy. *Cancer Control* **28** 10732748211041243. (<https://doi.org/10.1177/10732748211041243>)
- Kregiel D 2012 Succinate dehydrogenase of *Saccharomyces cerevisiae* – the unique enzyme of TCA cycle – current knowledge and new perspectives. In *Dehydrogenases*. London, UK: InTech. (<https://doi.org/10.5772/48413>)
- Lenders JW, Eisenhofer G, Mannelli M & Pacak K 2005 Pheochromocytoma. *Lancet* **366** 665–675. ([https://doi.org/10.1016/S0140-6736\(05\)67139-5](https://doi.org/10.1016/S0140-6736(05)67139-5))
- Letouze E, Martinelli C, Lorient C, Burnichon N, Abermil N, Ottolenghi C, Janin M, Menara M, Nguyen AT, Benit P, *et al.* 2013 SDH mutations establish a hypermethylator phenotype in paraganglioma. *Cancer Cell* **23** 739–752. (<https://doi.org/10.1016/j.ccr.2013.04.018>)
- Li F, He X, Ye D, Lin Y, Yu H, Yao C, Huang L, Zhang J, Wang F, Xu S, *et al.* 2015 NADP⁺-IDH mutations promote hypersuccinylation that impairs mitochondria respiration and induces apoptosis resistance. *Molecular Cell* **60** 661–675. (<https://doi.org/10.1016/j.molcel.2015.10.017>)
- Liao PC, Yang EJ & Pon LA 2020 Live-cell imaging of mitochondrial redox state in yeast cells. *STAR Protocols* **1** 100160. (<https://doi.org/10.1016/j.xpro.2020.100160>)
- Liu Y, Pang Y, Zhu B, Uher O, Caisova V, Huynh TT, Taieb D, Vanova KH, Ghayee HK, Neuzil J, *et al.* 2020 Therapeutic targeting of SDHB-mutated pheochromocytoma/paraganglioma with pharmacologic

- ascorbic acid. *Clinical Cancer Research* **26** 3868–3880. (<https://doi.org/10.1158/1078-0432.CCR-19-2335>)
- Loenarz C & Schofield CJ 2011 Physiological and biochemical aspects of hydroxylations and demethylations catalyzed by human 2-oxoglutarate oxygenases. *Trends in Biochemical Sciences* **36** 7–18. (<https://doi.org/10.1016/j.tibs.2010.07.002>)
- Lohr J & Acara M 1990 Effect of dimethylaminoethanol, an inhibitor of betaine production, on the disposition of choline in the rat kidney. *Journal of Pharmacology and Experimental Therapeutics* **252** 154–158.
- Lussey-Lepoutre C, Buffet A, Morin A, Goncalves J & Favier J 2018 Rodent models of pheochromocytoma, parallels in rodent and human tumorigenesis. *Cell and Tissue Research* **372** 379–392. (<https://doi.org/10.1007/s00441-018-2797-y>)
- Macarron R, Banks MN, Bojanic D, Burns DJ, Cirovic DA, Garyantes T, Green DVS, Hertzberg RP, Janzen WP, Paslay JW, *et al.* 2011 Impact of high-throughput screening in biomedical research. *Nature Reviews: Drug Discovery* **10** 188–195. (<https://doi.org/10.1038/nrd3368>)
- Malanga G, Aguiar MB, Martinez HD & Puntarulo S 2012 New insights on dimethylaminoethanol (DMAE) features as a free radical scavenger. *Drug Metabolism Letters* **6** 54–59. (<https://doi.org/10.2174/187231212800229282>)
- Marcer D & Hopkins SM 1977 The differential effects of meclufenoxate on memory loss in the elderly. *Age and Ageing* **6** 123–131. (<https://doi.org/10.1093/ageing/6.2.123>)
- Matlac DM, Hadrava Vanova K, Bechmann N, Richter S, Folberth J, Ghayee HK, Ge GB, Abunimer L, Wesley R, Aherrahour R, *et al.* 2021 Succinate mediates tumorigenic effects via succinate receptor 1: potential for new targeted treatment strategies in succinate dehydrogenase deficient paragangliomas. *Frontiers in Endocrinology* **12** 589451. (<https://doi.org/10.3389/fendo.2021.589451>)
- Miyazaki H, Nambu K, Minaki Y, Hashimoto M & Nakamura K 1976 Comparative studies on the metabolism of β -dimethylaminoethanol in the mouse brain and liver following administration of β -dimethylaminoethanol and its p-chlorophenoxyacetate, meclufenoxate. *Chemical and Pharmaceutical Bulletin* **24** 763–769. (<https://doi.org/10.1248/cpb.24.763>)
- Müller S, Sindikubwabo F, Cañeque T, Lafon A, Versini A, Lombard B, Loew D, Wu TD, Ginestier C, Charafe-Jauffret E, *et al.* 2020 CD44 regulates epigenetic plasticity by mediating iron endocytosis. *Nature Chemistry* **12** 929–938. (<https://doi.org/10.1038/s41557-020-0513-5>)
- Neumann HPH, Pawlu C, Pęczkowska M, Bausch B, McWhinney SR, Muresan M, Buchta M, Franke G, Klisch J, Bley TA, *et al.* 2004 Distinct clinical features of paraganglioma syndromes associated With SDHB and SDHD gene mutations. *JAMA* **292** 943–951. (<https://doi.org/10.1001/jama.292.8.943>)
- Niemann S & Müller U 2000 Mutations in SDHC cause autosomal dominant paraganglioma, type 3. *Nature Genetics* **26** 268–270. (<https://doi.org/10.1038/81551>)
- Pavlova NN & Thompson CB 2016 The emerging hallmarks of cancer metabolism. *Cell Metabolism* **23** 27–47. (<https://doi.org/10.1016/j.cmet.2015.12.006>)
- Peters JP, Her YF & Maher III LJ 2015 Modeling dioxygenase enzyme kinetics in familial paraganglioma. *Biology Open* **4** 1281–1289. (<https://doi.org/10.1242/bio.013623>)
- Petkov VD, Stancheva SL, Tocuschieva L & Petkov VV 1990 Changes in brain biogenic monoamines induced by the nootropic drugs adafenoxate and meclufenoxate and by citicholine (experiments on rats). *General Pharmacology: The Vascular System* **21** 71–75. ([https://doi.org/10.1016/0306-3623\(90\)90598-G](https://doi.org/10.1016/0306-3623(90)90598-G))
- Rijken JA, van Hulsteijn LT, Dekkers OM, Niemeijer ND, Leemans CR, Eijkelenkamp K, van der Horst-Schrivers ANA, Kerstens MN, van Berkel A, Timmers HJLM, *et al.* 2019 Increased mortality in SDHB but not in SDHD pathogenic variant carriers. *Cancers* **11** 103. (<https://doi.org/10.3390/cancers11010103>)
- Roy D & Singh R 1983 Age-related changes in glucose-6-phosphate dehydrogenase and 6-phosphogluconate dehydrogenase in the subcellular fractions from the rat brain and the effect of dimethylaminoethanol. *Biochemistry International* **7** 43–53.
- Saffi J, Sonego L, Varela QD & Salvador M 2006 Antioxidant activity of L-ascorbic acid in wild-type and superoxide dismutase deficient strains of *Saccharomyces cerevisiae*. *Redox Report* **11** 179–184. (<https://doi.org/10.1179/135100006X116691>)
- Selak MA, Armour SM, MacKenzie ED, Boulahbel H, Watson DG, Mansfield KD, Pan Y, Simon MC, Thompson CB & Gottlieb E 2005 Succinate links TCA cycle dysfunction to oncogenesis by inhibiting HIF- α prolyl hydroxylase. *Cancer Cell* **7** 77–85. (<https://doi.org/10.1016/j.ccr.2004.11.022>)
- Smestad J, Hamidi O, Wang L, Holte MN, Khazal FA, Erber L, Chen Y & Maher LJ 2017 Characterization and metabolic synthetic lethal testing in a new model of SDH-loss familial pheochromocytoma and paraganglioma. *Oncotarget* **9** 6109–6127. (<https://doi.org/10.18632/oncotarget.23639>)
- Smestad J, Erber L, Chen Y & Maher LJ 2018 Chromatin succinylation correlates with active gene expression and is perturbed by defective TCA cycle metabolism. *iScience* **2** 63–75. (<https://doi.org/10.1016/j.isci.2018.03.012>)
- Smith EH, Janknecht R & Maher LJ 2007 Succinate inhibition of α -ketoglutarate-dependent enzymes in a yeast model of paraganglioma. *Human Molecular Genetics* **16** 3136–3148. (<https://doi.org/10.1093/hmg/ddm275>)
- Warburg O 1956 On the origin of cancer cells. *Science* **123** 309–314. (<https://doi.org/10.1126/science.123.3191.309>)
- Weber D, Davies MJ & Grune T 2015 Determination of protein carbonyls in plasma, cell extracts, tissue homogenates, isolated proteins: focus on sample preparation and derivatization conditions. *Redox Biology* **5** 367–380. (<https://doi.org/10.1016/j.redox.2015.06.005>)
- Xiao M, Yang H, Xu W, Ma S, Lin H, Zhu H, Liu L, Liu Y, Yang C, Xu Y, *et al.* 2012 Inhibition of α -KG-dependent histone and DNA demethylases by fumarate and succinate that are accumulated in mutations of FH and SDH tumor suppressors. *Genes and Development* **26** 1326–1338. (<https://doi.org/10.1101/gad.191056.112>)
- Yoshioka S, Aso Y & Uchiyama M 1987 Kinetics of hydrolysis of meclufenoxate hydrochloride in human plasma. *Journal of Pharmacy and Pharmacology* **39** 215–218. (<https://doi.org/10.1111/j.2042-7158.1987.tb06251.x>)
- Zhang JH, Chung TDY & Oldenburg KR 1999 A simple statistical parameter for use in evaluation and validation of high throughput screening assays. *Journal of Biomolecular Screening* **4** 67–73. (<https://doi.org/10.1177/108705719900400206>)
- Zhang J, van den Herik BM & Wahl SA 2020 Alpha-ketoglutarate utilization in *Saccharomyces cerevisiae*: transport, compartmentation and catabolism. *Scientific Reports* **10** 12838. (<https://doi.org/10.1038/s41598-020-69178-6>)
- Zuckerman BM & Barrett KA 1978 Effects of pca and dmae on the nematode *Caenorhabditis briggsae*. *Experimental Aging Research* **4** 133–139. (<https://doi.org/10.1080/03610737808257136>)

Received in final form 11 February 2022

Accepted 21 March 2022

Accepted Manuscript published online 22 March 2022